COMMUNICATION

InP/ZnS Quantum Dots Photoluminescence Modulation via in situ H_2S Interface Engineering

Received 00th January 20xx,
Accepted 00th January 20xx

DOI: 10.1039/x0xx00000x

Xiang-Bing Fan,[a] Dong-Wook Shin,[a] Sanghyo Lee,[a] Junzhi Ye,[b] Shan Yu,[c] David J. Morgan,[d] Adrees Arbab,[a] Jiajie Yang,[a] Jeong-Wan Jo,[a] Yoonwoo Kim,[a] Sung-Min Jung,[a] Philip R. Davies,[c] Akshay Rao,[b] Bo Hou,[e] and Jong Min Kim[a]*

InP quantum dots (QDs) are attracting significant interest as a potentially less toxic alternative to Cd-based QDs in many research areas. Although InP-based core/shell QDs with excellent photoluminescent properties have been reported so far, sophisticated interface treatment to eliminate defects is often necessary. Herein, using aminophosphine as a seeding source of phosphorus, we find that H_2S can be efficiently generated from the reaction between thiol and alkylamine at high temperature. Apart from general comprehending that H_2S act as an S precursor, it is revealed that with core etching by H_2S, the interface between InP and ZnS can be reconstructed with S^{2-} incorporation. Such a transition layer can reduce inherent defects at the interface, resulting in significant photoluminescence (PL) enhancement. Meanwhile, the size of InP core could be further controlled by H_2S etching, which offers a feasible process to obtain wide band gap InP-based QDs with blue emission.

Introduction

With unique optoelectronic properties stemming from nanoscale dimensions,[1] quantum dots (QDs) are emerging semiconductor materials that underpin the development of future photonics and electronics applications including lighting,[2, 3] display,[4, 5] photovoltaic,[6] photosynthesis,[7] and biosensing.[8] Environmentally friendly indium phosphide (InP) based QDs (Cd/Pb-free), with a direct bandgap in the visible light region, tuneable emission bandwidth, and practicable material stability,[9, 10] have become strong candidates to achieve breakthroughs in the aforementioned fields. For example, InP-based QDs have been recently used as photoluminescent materials in the liquid crystal display market.[11] Latest advances in InP QDs light-emitting diode (LED) are pushing this research field to a next-generation self-emissive QD-LED display.[3, 12-16]

Nevertheless, because of the difficulties such as covalent In-P bond formation, highly reactive to be oxidized, and lack of green precursors,[9] the development of InP QDs synthesis has lagged behind that of related II-VI materials such as CdSe QDs. It is generally agreed that InP QDs with high PL could be realized by the protection of external ZnSe and ZnS shells. However, the photoluminescence quantum yield (PLQY) varies from 20% to near 100% for InP core/shell QDs dependent on different core and shell growth methods.[9, 13, 17-20] It has been reported that the defects from oxidative species and the lattice mismatch at the interface are probably the reasons for poor PL of InP core/shell QDs.[13, 17, 21, 22] Consequently, additional interface treatments such as HF etching of InP core are used to achieve high photoluminescent InP-based QDs.[13, 23] However, the harsh and complicated processing may hinder QDs large-scale production for future optoelectronic applications.

Here we propose a straightforward synthetic route to grow highly photoluminescent InP/ZnS QDs based on a facile interface engineering by in situ generated H_2S from thiol and alkylamine at high temperatures. It is revealed that an adequate amount of highly reactive H_2S can etch the InP core and create a transition layer at the interface, effectively eliminating the inherent interface defects and relaxing the lattice strain during the shell growth, which leads to PL enhancement. Furthermore, the in situ H_2S treatment also offers additional size controllability of the InP core, which opens more possibilities for the emission wavelength of InP-based QDs.

Results and Discussion

Synthesis and optical characterization

Two growth steps were implemented to synthesize InP/ZnS QDs: i) InP core QDs were prepared by the aminophosphine route with different ratios of $ZnCl_2$ and ZnI_2 to tune the InP core size;[24, 25] ii) ZnS shell was grown on the InP core by direct injection of zinc stearate ($ZnSt_2$) as Zn precursor and 1-dodecanethiol (DDT) as S precursor, followed by raising the temperature to 300 °C and kept for 60 min (see details in SI).

[a] Department of Engineering, University of Cambridge, Cambridge, CB3 0FA, UK. *E-mail: jmk71@cam.ac.uk
[b] The Cavendish Laboratory, Department of Physics, University of Cambridge, Cambridge, CB3 0HE, UK.
[c] School of New Energy and Materials, Southwest Petroleum University, Chengdu, 610500, China
[d] School of Chemistry, Cardiff University, Cardiff, CF10 3AT, UK
[e] School of Physics and Astronomy, Cardiff University, Cardiff, CF24 3AA, UK
[f] Electronic Supplementary Information (ESI) available: DOI: 10.1039/x0xx00000x

The absorption and PL spectra of InP and InP/ZnS QDs are shown in Figure 1. The absorption increase in the ultraviolet region confirmed ZnS shell formation (Figure S1A).[25] Interestingly, we find that after shell growth on the InP core, the absorption peak of InP/ZnS QDs was largely blue shifted from 505 nm to 470 nm (Figure 1A), which shows an abnormal behaviour to the optical properties of previously reported InP/ZnS QDs where PL peaks are nearly unchanged or a little red shifted.[24-26] This blueshift was also observed in the PL spectrum, with a peak at 521 nm of InP/ZnS QDs for green emission (Figure 1B). Compared to the poor PL from the InP QDs (PLQY ~1%), the PLQY increased to 85% after ZnS shell coating (Figure S1B), which is among the best results for InP/ZnS QDs synthesized from either tris(trimethylsilyl)-phosphine ($(TMS)_3P$) or aminophosphine.[18, 19, 25, 27] During the temporal shell growth process, the increase of PLQY was correlated with the blueshift of PL peak at high temperature (Figures S1C, S1D).

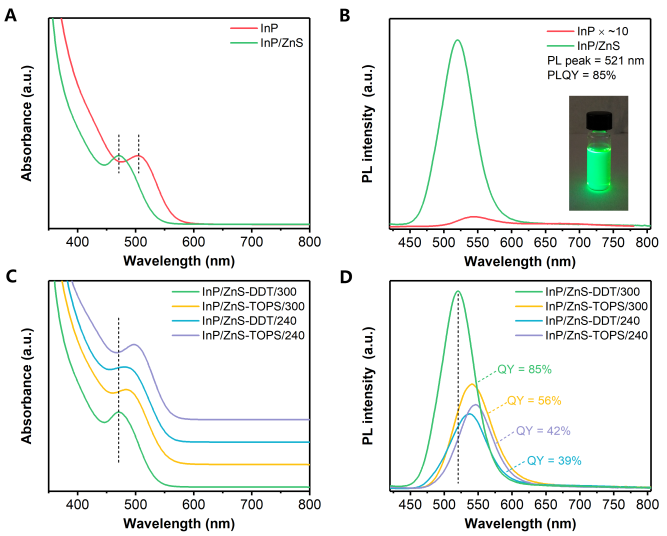

Figure 1. Optical properties of InP QDs and InP/ZnS QDs synthesized under different conditions. Absorption (A) and PL spectra (B) of InP and InP/ZnS QDs, the inset is the photograph of InP/ZnS QDs solution under UV light. Absorption (C) and PL spectra (D) of InP/ZnS QDs synthesized under different shell growth conditions.

Next, we investigated various shell growth parameters by changing precursors and reaction temperatures (Figures 1C, 1D). Initially, sulfur powder dissolved in trioctylphosphine as a common S precursor (TOPS) was employed for ZnS shell growth.[18, 24, 25] The PLQY of InP/ZnS QDs synthesized with TOPS was only 56% (Figure 1D). Compared to InP core QDs, peaks blueshift of InP/ZnS QDs with TOPS was also observed (absorption peak 484 nm, PL peak 541 nm), but much weaker than those with DDT reacted at 300 °C. Considering the lower PLQY may be caused by the different roles and reactivities between TOPS and DDT, the synthesis parameters when using TOPS were further modified. However, as shown in Figures S2A, S2C, changing the mole of TOPS precursor or prolonging the shell growth time could hardly obtain a comparable PLQY for InP/ZnS QDs.

Subsequently, to control the reactivity of precursors with DDT and $ZnSt_2$, the shell growth temperature varied from 210 to 300 °C in the presence of DDT (Figure S2B). Even though DDT can decompose and form ZnS shell between 200 °C to 240 °C according to previous literature for InP QDs synthesis,[27, 28] such a temperature range did not show high PL in our case (PLQY 39%, PL peak 537 nm). With a longer reaction time, the PLQY of InP/ZnS QDs synthesized with DDT at 240 °C still could not exceed 50% (Figure S2C). As the lower temperature with a longer reaction time cannot achieve desired PLQY, we believe the reaction process at a high temperature of 300 °C is significantly essential for obtaining high PLQY QDs. Furthermore, by introducing DDT after the TOPS reaction at 300 °C, the PLQY of InP/ZnS QDs was around 67% (Figure S2D). However, it is still lower than that of directly synthesized InP/ZnS QDs with DDT. Based on these experiments, we exclude the key role of DDT as additional surface ligands for achieving higher PLQY.

Surprisingly, we find that the value of PLQY was correlated with the extent of PL peak blueshift. When using TOPS or DDT at a lower temperature, lower PLQY was always associated with less peak movement compared to InP/ZnS-DDT/300 QDs. It is therefore important to understand how this peak shift happens. Accordingly, DDT or $ZnSt_2$, which existed in InP/ZnS-DDT/300 QDs synthesis, were introduced individually. The results show that DDT was critical for the blueshift of PL peak with increased PLQY, while the addition of $ZnSt_2$ alone yielded a small redshift for PL peak with limited PLQY improvement (Figure S3A). Such results exclude the possibility that Zn carboxylic precursor causes the blueshift with acid corrosion or water formation on the InP core.[30, 31] Moreover, a moderately excessive amount of DDT to $ZnSt_2$ in the system benefited PLQY (Figure S3B), and other thiols and zinc carboxylic with different aliphatic chains provided similar PL properties compared to the typical InP/ZnS-DDT/300 QDs synthesis (Figure S3C).

Finally, we repeated the synthesis of InP/ZnS-DDT/300 QDs to confirm the reproducibility of the proposed method, resulting in PLQY 84% ± 3 (highest 87%) for different batches with negligible peak wavelength variation (Figure S4A). The reproducibility is due to the simple and convenient synthesis procedure since it avoids elaborate precursor preparation, complicated interface treatment, like HF etching, and multiple core or shell growths. The obtained InP/ZnS QDs had good stability with PLQY maintained over one year (Figure S4B), demonstrating excellent protection of the InP core by the ZnS shell.

Structure and component characterization

In general, the blueshift of absorption and PL spectra of QDs can be caused by the formation of new core compounds,[32] Zn doping in the core,[33] and size decrease or morphology change with increased quantum confinement effect.[34] X-ray diffraction patterns (XRD; Figure 2A) reveal the InP QDs have zinc blende structure. Upon shell growth, the peaks shift to higher angle from InP to ZnS.[25] TEM images show that the morphology for both InP and InP/ZnS QDs were quasi-spherical (Figure S5). Based XRD and TEM results, no other side products can be indentified. The size of the as-prepared InP core was about 2.5 nm (Figure S6), which is close to the literature data.[23, 35] For

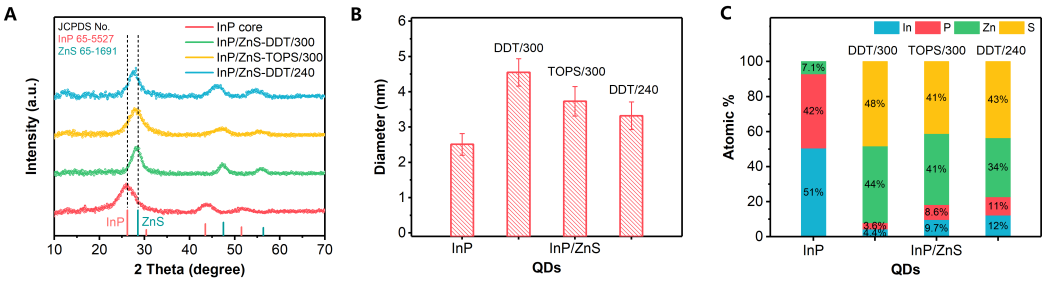

Figure 2. Structure and component characterization of InP cores and InP/ZnS QDs synthesized under different conditions. (A) XRD patterns of InP and InP/ZnS QDs. (B) TEM size distributions of InP and InP/ZnS QDs. (C) Elemental composition results by ICP-OES of InP and InP/ZnS QDs.

InP/ZnS-DDT/300 QDs, the QDs size increased to 4.6 nm, larger than InP/ZnS-TOPS/300 QDs (3.7 nm) and InP/ZnS-DDT/240 QDs (3.3 nm). HRTEM image for InP/ZnS-DDT/300 QDs (Figure S6) shows the interplanar spacing as 0.319 nm, which is between the (111) facet of zinc blende InP (0.339 nm) and ZnS (0.312 nm). Elemental analysis of QDs by inductively coupled plasma optical emission spectrometry (ICP-OES; Figure 2C, Table S1) and scanning electron microscope energy dispersive X-ray spectroscopy (SEM-EDS; Table S2) presented similar ratios of P to In (0.8-0.9) for all the QDs. The similar P to In ratios in the InP/ZnS QDs suggest the blueshift of the peak wavelength does not result from a large amount of Zn replacing In and alloying into the InP core.[33]

Alternatively, a size decrease of the InP core might happen during shell growth, especially for the reaction with DDT at 300 °C. We notice that H_2S can be generated in situ by DDT and Oleylamine (OLA) at high temperatures.[35] Thus we focused on the appearance of H_2S in our shell growth processes. To verify H_2S gas generation, a Pb^{2+} aqueous solution was used and resulting in black PbS precipitates (Figure 3A).[37] It is noticed that the black precipitates started appearing after the temperature was raised above 250 °C, and a large amount of precipitate was observed at the end of the reaction (Figures 3A, 3B). EDS and XRD further confirmed the PbS black precipitates (Figure S7), indicating the formation of H_2S during the shell growth by DDT at 300 °C. H_2S is an acidic gas and can etch InP structure,[37] resulting in a size decrease of the InP core that contributed to the blueshift of absorption and PL spectra. In other shell growth processes such as TOPS at 300 °C or lower temperature with DDT at 240 °C, the Pb^{2+} solutions became slightly darker but remained transparent (Figures 3D, 3E), indicating a small amount of H_2S release in these conditions. Besides DDT and high temperature, we find that OLA is also necessary for the efficient H_2S generation. If OLA was removed or replaced by a carboxylic acid such as oleic acid (OA), the generation of H_2S was also minimized (Figures S8B, S8C).

To further confirm the in situ generation of H_2S, gas chromatography with flame photometric detector (GC-FPD) was used to monitor the possible gas generation during the reaction.[39] The gas was extracted from the reaction flask, injected into the GC-FPD, and then compared with standard H_2S gas. It can be clearly seen the reaction flask contact H_2S gas with retention time (RT) = 1.5 min (Figure 3E). While some other S-contained gas, such as carbonyl sulfide (COS, RT ~ 1.7 min), methanethiol (CH_3SH, RT ~ 2.3 min), ethanethiol (C_2H_5SH, RT ~ 3.7 min), and carbon disulfide (CS2, RT ~ 4.3 min), were not detected in the reaction system. We further monitored the H_2S generation during the shell growth process with different heating times (Figure 3F). It shows H_2S was largely generated when the temperature reached 300 °C and the amount of H_2S was gradually increased as the heating time went on. Besides, we also compared H_2S generation by GC-FPD with the different shell growth conditions (Figure 3G), which show that H_2S generation with DDT at 300 °C is much higher than those in other conditions including DDT at 240 °C, TOPS at 300 °C and TOPS at 240 °C. Such results accord well with the finding in H_2S detection with Pb^{2+} solution above.

Although in situ generation of H_2S by some other recipes in QDs synthesis has been reported, most works focus on H_2S as an S resource.[37, 40-42] The significant role of H_2S over other S precursors for higher PLQY is still unclear. To understand the chemical change in the InP surface composition, X-ray photoelectron spectroscopy (XPS) was employed. From In 3d spectra, we find a peak shift for InP/ZnS-DDT/300 QDs compared to the others (Figure 4A), indicating a different chemical environment of In after exposure to a large amount of H_2S. Considering the high reactivity of H_2S with InP, the peak shift to higher binding energy probably occurred from the contribution of newly formed In-S bonds at the interface.[38, 41] A further peak deconvolution for In $3d_{5/2}$ spectrum shows that two peaks with 444.6 eV and 445.2 eV are well fitted to the spectrum (Figure S8A), where the former 444.6 eV comes from

In-P bonds, and the latter 445.2 eV matches the binding energy of P-In-S bonds in the literature.[43] For other QDs, there is still an In 3d peak shift compared to the In-P value (Figure S8A). This smaller peak shift can be assigned to In-O bonds or fewer In-S bonds.[31, 44, 45] For the InP/ZnS QDs synthesized in the absence of H_2S (InP/ZnS-TOPS/300 and InP/ZnS-DDT/240 QDs), the interface treatment also occurred, mainly from the reaction between the InP core with H_2O generated by the side reaction of carboxylic acid during the shell growth process.[17, 31] However, the H_2O generation is much slower and insufficient in these conditions, resulting in an inadequate interface layer.

The XPS P 2p spectra were also measured and show two chemical environments for P for QDs (Figure 4B): i) the peak at around 129 eV is characteristic of reduced P (P^{-3}) in InP; ii) The peak at 133-134 eV is indicative of a positive oxidation state as either P^{3+} or P^{5+}. For the InP core QDs without shell protection, the surface of the InP core was easily oxidized by O_2 and H_2O during QDs synthesis or purification, resulting in P^{3+}/P^{5+} compounds.[17, 46] For InP/ZnS QDs, we find that the P^{3+}/P^{5+} in InP/ZnS-DDT/300 QDs (67% ratio of P^{3+}/P^{5+} to all P) is much

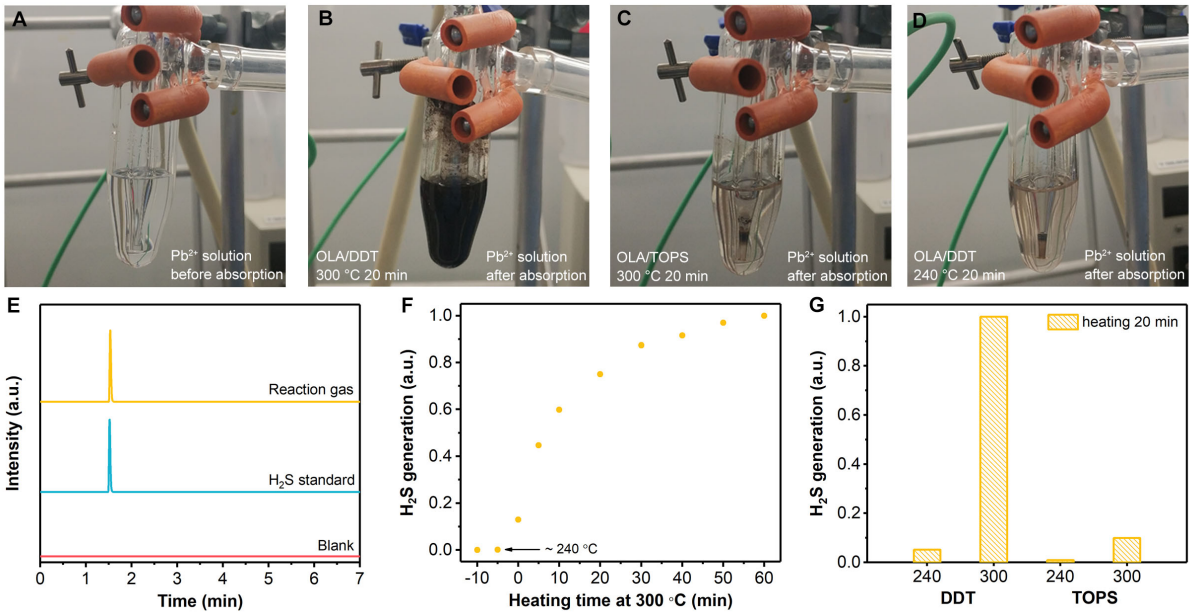

Figure 3. (A-D) Detection of H_2S gas generation by Pb^{2+} solution. Pb^{2+} absorption: 20 mg/mL $Pb(Ac)_2{\cdot}2H_2O$ aqueous solution. (A) Pb^{2+} solution before reaction. (B-D) Pb^{2+} solution under different reaction conditions: (B) OLA/DDT at 300 °C, (C) OLA/TOPS at 300 °C, (D) OLA/DDT at 240 °C. (E-F) Detection of H_2S gas generation by GC-FPD. (E) Comparison between the gas extract from flask, H_2S standard gas (H_2S in Ar) and blank (Ar). (F) Time monitoring of H_2S gas generation from DDT and OLA during heating at 300 °C. The time before 0 min represents the heat up period. (G) Comparison of H_2S generation at different reaction conditions.

higher than that in other shell growth conditions (37-51%). Considering the highest PLQY observed at InP/ZnS-DDT/300 QDs, our finding indicates that the content of oxidized phosphorous at the interface has no direct correlation with the PLQY of InP/ZnS QDs, which differs from a recent report that claims oxide-free phosphorus interface is beneficial for higher PLQY of InP QDs.[13] As shown in Figure S8B, fitting of the P $2p_{3/2}$ spectra at 133-134 eV shows the peak for InP/ZnS-DDT/300 QDs at a binding energy of 133.7 eV, which is higher than that of InP/ZnS-TOPS/300 and InP/ZnS-DDT/240 QDs (133.4 eV). Based on our observation and literature reports,[38, 41, 47] the increased oxidization of P (P^{3+}/P^{5+}) in InP/ZnS-DDT/300 QDs was contributed from the efficient H_2S reaction by core etching and interface reconstruction, probably with some P-S bonds.[38, 47, 48] Besides, the XPS of Zn 3d for all QDs were nearly the same (Figure S9A), showing that this interface engineering with H_2S barely influenced the ZnS shell. Furthermore, we do not observe any sulfur oxidation around 168-169 eV in the S 2p spectra (Figure S9B). The slight peak shift for QDs with DDT was mainly attributed to the different S resources, where thiols have higher binding energy than inorganic sulfide.[42]

Photophysical study

Next, photophysical studies of InP and InP/ZnS QDs were conducted to understand the internal relationship between interface states and photoluminescence. Generally, dynamic decays in a very short time (< 100 ps) are relevant to inherent defects, while longer decay processes (~ns) are derived from surface traps.[49, 50] Time-resolved photoluminescence (TRPL) spectra by time-correlated single-photon counting (TCSPC) firstly show the dynamic decay of PL in the nanosecond range (Figure 5A). The longer PL lifetime of InP/ZnS QDs compared to InP QDs is well understood, as excitons can be effectively isolated from the core surface after shell coating. Therefore, the fast decay process by nonradiative recombination of charge carriers occurred at the surface of InP core was largely suppressed, and PLQY was improved with slower dynamic decay.[49, 51] However, no significant difference in the TRPL curves was observed among these InP/ZnS QDs, with similar average lifetimes around 75-80 ns (Figure 5A, Table S3), implying that surface trapping is not the only factor for the different PLQY of

QDs. This is also consistent with that some InP-based QDs with very thick shells and slow

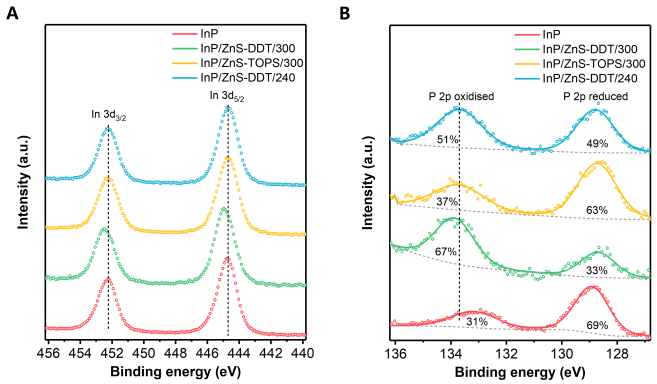

Figure 4. X-ray photoelectron spectroscopy profiles of InP cores and InP/ZnS QDs synthesized under different conditions. (A) In 3d spectra of InP and InP/ZnS QDs. (B) P 2p spectra of InP and InP/ZnS QDs, the value inside the peak is the percentage of oxidized and reduced P.

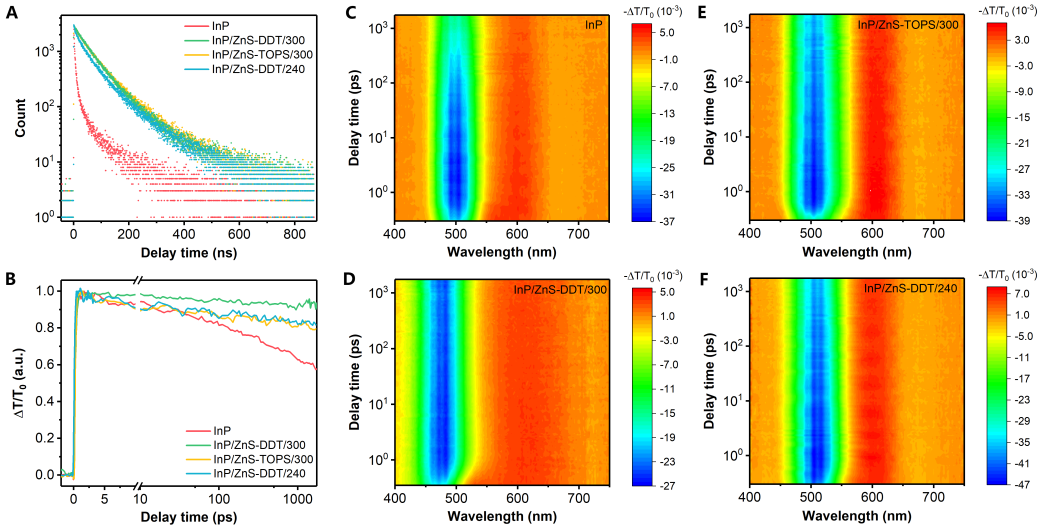

Figure 5. Photophysical study of InP cores and InP/ZnS QDs synthesized under different conditions. (A) Time-resolved photoluminescence spectra of InP and InP/ZnS QDs. (B) TA kinetics spectra for excitation bleaching signal (average from peaks ± 10 nm) of InP and InP/ZnS QDs. (C-F) TA mapping of InP and InP/ZnS QDs in different wavelengths and delay times.

TRPL decay in nanosecond range have modest PLQY (below 50%),[17, 35, 52] even though the thick shell can keep wave functions of excitons away from the surface of QDs.[15, 18]

Furthermore, the QDs were characterized by ultrafast transient absorption (TA) spectra in the picosecond range. All the TA spectra of InP/ZnS QDs (Figure 5C-5F) display two prominent features, typical excitation photo-bleaching and featureless broad photoinduced absorption. Unlike the similarity of decay in the nanosecond range, InP/ZnS QDs with TOPS/300 and DDT/240 show a faster recovery of excitation bleaching than InP/ZnS-DDT/300 QDs (Figure 5B), indicating an ultrafast recombination process in the picosecond time range. Fast exciton decays are normally relevant to inherent defects,[49, 50] therefore, the ultrafast recombination in QDs with TOPS/300 and DDT/240 can be attributed to inherent defects in the QDs, which are mainly at the surface/interface or inside the InP core. We believe the superiority high PLQY of as-prepared InP/ZnS-DDT/300 QDs could be attributed to their fewer inherent defects.

Due to large lattice mismatch between InP and ZnS, the inherent defects will be formed at the interface by growing ZnS shell on InP core, especially without any transition layer that leads to a very low PLQY.[21] For general InP/ZnS QDs synthesis, the interface treatment by side reactions is not efficient enough to remove the interface defects. Unlike the external surface traps that can be isolated by increasing shell thickness, the inherent defects at the interface still exist after shell growth, which leads to moderate PLQY of QDs.[17, 31] Differently, the in situ H_2S generation can provide abundant highly reactive H_2S to the surface of InP core in a short time. Therefore, the pristine InP surface structure can be etched and reconstructed with S^{2-} incorporation, accompanied by the decrease of InP core size. Following by the growth of ZnS shell, this transition layer could reduce the interface defects, relax the lattice strain and lead to extended conformal ZnS shell growth.[53] This hypothesis can also explain the thicker shell and more regular shape observed in TEM for InP/ZnS-DDT/300 QDs.

The above analysis may decipher the apparent contradiction that some higher PL InP QDs synthesis turns out to contain more

P in a positive oxidation state,[21, 23, 54] despite the supposition that P^{3+}/P^{5+} free InP core benefit for high PLQY.[9, 13] From our result, the H_2S interface engineering with more oxidized P can also reduce the interface defects, resulting in improvement of PLQY. Therefore, we assume that rather than oxidation states, introducing a highly reactive chemical is more crucial to reconstructing the interface with fewer inherent defects for high PLQY QDs synthesis, which includes previous reported HF,[13, 23, 55], ZnF_2,[20] $(NH_4)_2S$,[56] or H_2S in this work.

Extended synthesis for QDs emission at different wavelengths.

The developed facile InP/ZnS QDs synthetic method based on H_2S interface engineering was well utilized to synthesize QDs with emission that covers the most range of visible light. Firstly, the PL peak wavelength of InP/ZnS QDs could be precisely controlled by changing the reaction temperature during InP core formation for different core sizes, varying from 500 to 550 nm with PLQY over or close to 80% (Figure 6A). As the InP/ZnS QDs synthesized with H_2S generation can get higher PLQY with similar emission wavelength for InP/ZnS-TOPS/300 and InP/ZnS-DDT/240 QDs, it further shows that the main contribution to PLQY from H_2S is interface engineering rather than just tuning the size or emission wavelength of InP core.

Secondly, significant InP size change and emission modulation to red, orange or blue could be realized by tuning different halogen precursors used at the beginning of the synthesis (see details in SI).[24, 25] Orange and red emissions of InP/ZnS QDs were obtained from $ZnCl_2$ precursor (Figure 6B), and blue emission of InP/ZnS QDs was synthesized from ZnI_2 precursor (Figures 6C). In particular, the InP/ZnS QDs at 468 nm with 54% PLQY (Figures 6C, S10A, S10B) provide a promising and feasible blue emission InP-based QDs synthesis approach, which shall be vital for QDs lighting and display application. Further studies show that blueshift in the PL spectrum was also observed during the shell growth (Figures S10C, S10D), which agrees with the green emission InP/ZnS QDs synthesis. Control experiments show that, without efficient generation of H_2S, the PL peaks of InP/ZnS QDs were located at the wavelength region for cyan emission (482 nm - 506 nm) with lower PLQY (Figure 6C). Moreover, introducing more DDT and $ZnSt_2$ for a second shell growth allowed PLQY to increase to 66% (Figure 6C). Although there have been several reports for InP-based QDs synthesis with blue emission,[45, 57, 58] the mechanism for obtaining short PL wavelength of InP-based QDs with high PLQY is still confused. Generally, the realization of a smaller InP core for blue emission conflicts with the effective elimination of defects. Due to the rapid nucleation process, small size of InP QDs should be obtained with a quick termination of the core formation, easily leaving a lot of unreacted species and trap states on the surface of InP core.[9] Furthermore, it is more difficult to achieve controllable epitaxial growth of shells for the smaller size of core QDs. Our finding shows that fine control of smaller InP size can be realized by getting a large core firstly, then reducing core size by H_2S etching, resulting in a shorter emission wavelength (i.e. blue region) with high PLQY.

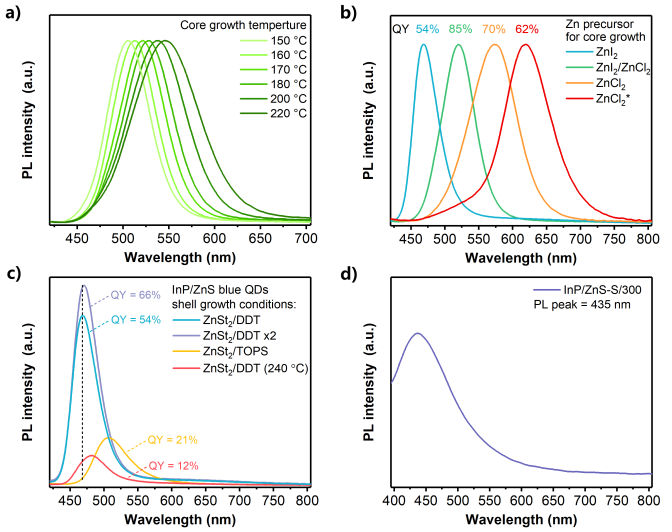

Figure 6. Extend synthesis of InP/ZnS QDs for different wavelength emissions. (A) PL spectra of green emission InP/ZnS QDs synthesized under different core formation temperatures. All PLQY of the InP/ZnS QDs is over 80% except for the InP core formation at 220 °C, where the PLQY is 75%. (B) PL spectra of InP/ZnS QDs with different Zn halide precursors used for the InP core formation. The red line is for aminophosphines injected twice. (C) PL spectra of blue emission InP/ZnS QDs synthesized under different shell growth conditions. (D) PL spectra for InP/ZnS QDs synthesized with $ZnSt_2$ and sulfur powder (8 mmol) for shell formation. The shell growth temperature is 300 °C.

The success of blue colour emission through H_2S generation inspires us to promote the PL of InP QDs to deep blue emission. However, it did not work well by further changing In and Zn precursors. Therefore, we developed another procedure to accelerate the reaction between H_2S and InP core by increasing H_2S generation rate. Instead of DDT/OLA or TOPS, we found that a combination of sulfur powder with OLA (S/OLA) can result in a much faster H_2S generation,[40, 59, 60] which enlarges the etching extent of the InP core. As shown in Figure 4d, a larger blueshift of PL to deep blue emission at 435 nm with PLQY around 18% is observed, which over-ranged the typical emission wavelength of reported InP-based QDs.[10] Elemental analysis confirms the structure of InP was partially maintained after the shell growth (Table S4). Although further optimization is needed, as-proposed photoluminescence modulation via in situ H_2S interface engineering has offered a strong promise for deep blue emission InP-based QDs synthesis.

Conclusions

In summary, we propose an easy strategy for photoluminescence modulation of InP-based QDs by in situ H_2S interface engineering. Comparison with different shell growth conditions confirms that H_2S can be generated at an appropriate rate from DDT and OLA at high temperature. The efficient H_2S etching with S^{2-} incorporation into the InP core causes interface reconstruction, reduces the inherent defects and relaxes the lattice strain at the interface during shell growth, leading to a higher PLQY of QDs. Furthermore, the in situ H_2S interface engineering can also offer an additional size control of InP core, which brings more possibilities for blue emission InP

QDs synthesis. We believe that as-proposed in situ H_2S generation approach can provide a convenient interface treatment strategy and enable an additional PL wavelength tunability, which shall have a significant impact on high-quality InP-based QDs and other nanocrystals synthesis.

Author Contributions

X.B.F., B.H., and J.M.K. conceived the idea, X.B.F., D.W.S., and S.L. designed the experiment. X.B.F., D.W.S., S.L., and J.J.Y. performed the QDs synthesis and characterization. J.Z.Y. and A.R. performed the femtosecond transient absorption measurement. D.J.M. and P.R.D. performed the XPS measurement. X.B.F., D.W.S., and S.Y., drafted the manuscript. All authors analyzed the data and commented on the manuscript. B.H., and J.M.K. supervised the work.

Acknowledgments

This work was supported by grants from European Commission Horizon 2020 (685758) and Engineering and Physical Sciences Research Council (EPSRC, EP/P027628/1). XPS data collection was performed at the EPSRC National Facility for XPS (HarwellXPS), operated by Cardiff University and UCL, under contract No. PR16195.

Conflicts of interest

There are no conflicts to declare.

References

1. A. L. Efros, *Nature*, 2019, **575**, 604-605.
2. Z. Yang, M. Gao, W. Wu, X. Yang, X. W. Sun, J. Zhang, H.-C. Wang, R.-S. Liu, C.-Y. Han, H. Yang and W. Li, *Mater. Today*, 2019, **24**, 69-93.
3. A. R. C. Osypiw, S. Lee, S.-M. Jung, S. Leoni, P. M. Smowton, B. Hou, J. M. Kim and G. A. J. Amaratunga, *Materials Advances*, 2022, **3**, 6773-6790.
4. Y. Shu, X. Lin, H. Qin, Z. Hu, Y. Jin and X. Peng, *Angew. Chem. Int. Ed.*, 2020, **59**, 22312-22323.
5. T. Meng, Y. Zheng, D. Zhao, H. Hu, Y. Zhu, Z. Xu, S. Ju, J. Jing, X. Chen, H. Gao, K. Yang, T. Guo, F. Li, J. Fan and L. Qian, *Nat. Photonics*, 2022, **16**, 297-303.
6. M. Yuan, M. Liu and E. H. Sargent, *Nat. Energy*, 2016, **1**, 16016.
7. X.-B. Li, C.-H. Tung and L.-Z. Wu, *Nat. Rev. Chem.*, 2018, **2**, 160-173.
8. K. D. Wegner and N. Hildebrandt, *Chem. Soc. Rev.*, 2015, **44**, 4792-4834.
9. S. Tamang, C. Lincheneau, Y. Hermans, S. Jeong and P. Reiss, *Chem. Mater.*, 2016, **28**, 2491-2506.
10. P. Reiss, M. Carriere, C. Lincheneau, L. Vaure and S. Tamang, *Chem. Rev.*, 2016, **116**, 10731-10819.
11. A. K. Srivastava, W. Zhang, J. Schneider, J. E. Halpert and A. L. Rogach, *Adv. Sci.*, 2019, **6**, 1901345.
12. J. Lim, M. Park, W. K. Bae, D. Lee, S. Lee, C. Lee and K. Char, *ACS Nano*, 2013, **7**, 9019-9026.
13. Y.-H. Won, O. Cho, T. Kim, D.-Y. Chung, T. Kim, H. Chung, H. Jang, J. Lee, D. Kim and E. Jang, *Nature*, 2019, **575**, 634-638.
14. Y. Li, X. Hou, X. Dai, Z. Yao, L. Lv, Y. Jin and X. Peng, *J. Am. Chem. Soc.*, 2019, **141**, 6448-6452.
15. E. Jang, Y. Kim, Y.-H. Won, H. Jang and S.-M. Choi, *ACS Energy Lett.*, 2020, **5**, 1316-1327.
16. Z. Wu, P. Liu, W. Zhang, K. Wang and X. W. Sun, *ACS Energy Lett.*, 2020, **5**, 1095-1106.
17. J. L. Stein, W. M. Holden, A. Venkatesh, M. E. Mundy, A. J. Rossini, G. T. Seidler and B. M. Cossairt, *Chem. Mater.*, 2018, **30**, 6377-6388.
18. D. Hahm, J. H. Chang, B. G. Jeong, P. Park, J. Kim, S. Lee, J. Choi, W. D. Kim, S. Rhee, J. Lim, D. C. Lee, C. Lee, K. Char and W. K. Bae, *Chem. Mater.*, 2019, **31**, 3476-3484.
19. B. Chen, D. Li and F. Wang, *Small*, 2020, **16**, 2002454.
20. H. Li, W. Zhang, Y. Bian, T. K. Ahn, H. Shen and B. Ji, *Nano Lett.*, 2022, **22**, 4067–4073.
21. M. D. Tessier, E. A. Baquero, D. Dupont, V. Grigel, E. Bladt, S. Bals, Y. Coppel, Z. Hens, C. Nayral and F. Delpech, *Chem. Mater.*, 2018, **30**, 6877-6883.
22. F. W. Eagle, N. Park, M. Cash and B. M. Cossairt, ACS Energy Lett., 2021, 6, 977-984.
23. Y.-C. Pu, H.-C. Fan, J.-C. Chang, Y.-H. Chen and S.-W. Tseng, *J. Phys. Chem. Lett.*, 2021, **12**, 7194-7200.
24. S. Yu, X.-B. Fan, X. Wang, J. Li, Q. Zhang, A. Xia, S. Wei, L.-Z. Wu, Y. Zhou and G. R. Patzke, *Nat. Commun.*, 2018, **9**, 4009.
25. M. D. Tessier, D. Dupont, K. De Nolf, J. De Roo and Z. Hens, *Chem. Mater.*, 2015, **27**, 4893-4898.
26. L. Li and P. Reiss, *J. Am. Chem. Soc.*, 2008, **130**, 11588-11589.
27. K. Nemoto, J. Watanabe, H.-T. Sun and N. Shirahata, *Nanoscale*, 2022, **14**, 9900-9909.
28. T. Kim, S. W. Kim, M. Kang and S.-W. Kim, *J. Phys. Chem. Lett.*, 2012, **3**, 214-218.
29. W.-S. Song, H.-S. Lee, J. C. Lee, D. S. Jang, Y. Choi, M. Choi and H. Yang, *J. Nanopart. Res.*, 2013, **15**, 1750.
30. E. Ryu, S. Kim, E. Jang, S. Jun, H. Jang, B. Kim and S.-W. Kim, *Chem. Mater.*, 2009, **21**, 573-575.
31. H. Virieux, M. Le Troedec, A. Cros-Gagneux, W.-S. Ojo, F. Delpech, C. Nayral, H. Martinez and B. Chaudret, *J. Am. Chem. Soc.*, 2012, **134**, 19701-19708.
32. V. Srivastava, V. Kamysbayev, L. Hong, E. Dunietz, R. F. Klie and D. V. Talapin, *J. Am. Chem. Soc.*, 2018, **140**, 12144-12151.
33. F. Pietra, L. De Trizio, A. W. Hoekstra, N. Renaud, M. Prato, F. C. Grozema, P. J. Baesjou, R. Koole, L. Manna and A. J. Houtepen, *ACS Nano*, 2016, **10**, 4754-4762.
34. A. M. Smith and S. Nie, *Acc. Chem. Res.*, 2010, **43**, 190-200.
35. K. Kim, D. Yoo, H. Choi, S. Tamang, J.-H. Ko, S. Kim, Y.-H. Kim and S. Jeong, *Angew. Chem. Int. Ed.*, 2016, **55**, 3714-3718.
36. D. Yoo, M. Kim, S. Jeong, J. Han and J. Cheon, *J. Am. Chem. Soc.*, 2014, **136**, 14670-14673.
37. Z. Li, Y. Ji, R. Xie, S. Y. Grisham and X. Peng, *J. Am. Chem. Soc.*, 2011, **133**, 17248-17256.
38. A. J. Nelson, S. Frigo and R. Rosenberg, *J. Appl. Phys.*, 1992, **71**, 6086-6089.
39. W. Wardencki and B. Zygmunt, Anal. Chim. Acta, 1991, 255, 1-13.
40. J. W. Thomson, K. Nagashima, P. M. Macdonald and G. A. Ozin, *J. Am. Chem. Soc.*, 2011, **133**, 5036-5041.
41. L. Xi, D.-Y. Cho, M. Duchamp, C. B. Boothroyd, J. Y. Lek, A. Besmehn, R. Waser, Y. M. Lam and B. Kardynal, *ACS Appl. Mater. Interfaces*, 2014, **6**, 18233-18242.

42. A. C. Berends, W. van der Stam, J. P. Hofmann, E. Bladt, J. D. Meeldijk, S. Bals and C. de Mello Donega, *Chem. Mater.*, 2018, **30**, 2400-2413.
43. K. Huang, R. Demadrille, M. G. Silly, F. Sirotti, P. Reiss and O. Renault, *ACS Nano*, 2010, **4**, 4799-4805.
44. H. Xu, Y. Wang, X. Dong, N. Zheng, H. Ma and X. Zhang, *Appl. Catal., B*, 2019, **257**, 117932.
45. Z. Cui, S. Mei, Z. Wen, D. Yang, S. Qin, Z. Xiong, B. Yang, H. He, R. Bao, Y. Qiu, Y. Chen, W. Zhang, F. Xie, G. Xing and R. Guo, *Small*, 2022, **18**, 2108120.
46. A. Buffard, S. Dreyfuss, B. Nadal, H. Heuclin, X. Xu, G. Patriarche, N. Mézailles and B. Dubertret, *Chem. Mater.*, 2016, **28**, 5925-5934.
47. K. Z. Liu, Y. Suzuki and Y. Fukuda, *Appl. Surf. Sci.*, 2004, **237**, 623-626.
48. M. Pelavin, D. N. Hendrickson, J. M. Hollander and W. L. Jolly, *J. Phys. Chem.*, 1970, **74**, 1116-1121.
49. W. Yang, Y. Yang, A. L. Kaledin, S. He, T. Jin, J. R. McBride and T. Lian, *Chem. Sci.*, 2020, **11**, 5779-5789.
50. K. E. Knowles, E. A. McArthur and E. A. Weiss, *ACS Nano*, 2011, **5**, 2026-2035.
51. K. Wu, N. Song, Z. Liu, H. Zhu, W. Rodríguez-Córdoba and T. Lian, *J. Phys. Chem. A*, 2013, **117**, 7561-7570.
52. K. R. Reid, J. R. McBride, N. J. Freymeyer, L. B. Thal and S. J. Rosenthal, *Nano Lett.*, 2018, **18**, 709-716.
53. M. Rafipoor, D. Dupont, H. Tornatzky, M. D. Tessier, J. Maultzsch, Z. Hens and H. Lange, *Chem. Mater.*, 2018, **30**, 4393-4400.
54. K. Kim, Y.-H. Suh, D. Kim, Y. Choi, E. Bang, B. H. Kim and J. Park, *Chem. Mater.*, 2020, **32**, 2795-2802.
55. T. Kim, K.-H. Kim, S. Kim, S.-M. Choi, H. Jang, H.-K. Seo, H. Lee, D.-Y. Chung and E. Jang, *Nature*, 2020, **586**, 385-389.
56. V. Sayevich, Z. L. Robinson, Y. Kim, O. V. Kozlov, H. Jung, T. Nakotte, Y.-S. Park and V. I. Klimov, *Nat. Nanotechnol.*, 2021, **16**, 673-679.
57. W. Shen, H. Tang, X. Yang, Z. Cao, T. Cheng, X. Wang, Z. Tan, J. You and Z. Deng, *J. Mater, Chem. C*, 2017, **5**, 8243-8249.
58. W. Zhang, S. Ding, W. Zhuang, D. Wu, P. Liu, X. Qu, H. Liu, H. Yang, Z. Wu, K. Wang and X. W. Sun, *Adv. Funct. Mater.*, 2020, **30**, 2005303.
59. B. Hou, D. Benito-Alifonso, R. Webster, D. Cherns, M. C. Galan and D. J. Fermín, J. Mater. Chem. A, 2014, 2, 6879-6886.
60. S.-Y. Yoon, J.-H. Kim, E.-P. Jang, S.-H. Lee, D.-Y. Jo, Y. Kim, Y. R. Do and H. Yang, *Chem. Mater.*, 2019, **31**, 2627-2634.

